Annals of Glaciology 33 2001
© International Glaciological Society

Modelling sea-ice thermodynamics in BALTEX-BASIS

Bin Cheng, Jouko Launiainen, Timo Vihma, Juha Uotila
Finnish Institute of Marine Research, P.O. Box 33, FIN-00931 Helsinki, Finland

ABSTRACT. In this paper, we present the results of a one-dimensional, thermodynamic sea-ice model applied to the Baltic Air–Sea–Ice Study (BASIS) field data. In general, the model results are in good agreement with the measurements, which were made during mild weather conditions with distinct areal and temporal variations in the snow and ice thickness. The total amount of refrozen ice calculated from the surface melting water gives a first-order estimate of snow-ice formation during the BASIS experiment, and this agreed well with the total observed variation in ice thickness. The model slightly overestimated ice growth at the bottom. This may be due to the variation in sea-ice thermal properties, affected by a slush layer between the snow and ice, or to the lack of ice–ocean interaction in the model.

INTRODUCTION

The Baltic Air–Sea–Ice Study (BASIS) is a sub-project of the Baltic Sea program BALTEX of the World Climate Research Programme/Global Energy and Water Cycle Experiment (WCRP/GEWEX). It is carried out by Finnish, Swedish and German institutes. Observations for validation and optimization of the thermodynamic ice model were performed during the BASIS field campaign in the northern Baltic Sea in 1998. The goals of the project include an investigation into air–ice–ocean coupling and its modelling (Launiainen, 1999).

A one-dimensional, multi-layer sea-ice model was created in the Finnish Institute of Marine Research (FIMR) to study ice thermodynamics and air–ice–sea coupling (Cheng and Launiainen, 1998; Launiainen and Cheng, 1998). Overall, the model is similar to those of Gabison (1987) and Ebert and Curry (1993). The main physical processes expressed in the model involve the air–ice coupling, heat fluxes and heat balance at the surface and the ice bottom, heat conduction in the multi-layer snow and ice, and mass balances at the surface and the bottom. The model is shown schematically in Figure 1. Model solutions are obtained using the following procedures:

(1) The turbulent air–ice fluxes of momentum, sensible and latent heat are calculated on the basis of Monin–Obukhov similarity theory. Integration of the non-dimensional universal profile gradients of wind speed (V), temperature (T) and moisture (q) yield the vertical profiles of $V(z_a)$, $T(z_a)$ and $q(z_a)$ in the surface boundary layer (SBL).

(2) Various heat fluxes, i.e. the net downward shortwave radiation $(1-\alpha)Q_s$, the shortwave absorption in snow and ice (I), the downward (Q_d) and upward (Q_b) longwave radiation, the sensible heat (Q_h), the latent heat (Q_{le}) and the surface conductive heat flux (F_c), are used to construct a heat- and mass-balance equation for the surface layer of ice or snow. This balance serves as the upper boundary condition needed to describe heat conduction in the ice. The surface temperature (T_{sfc}) is the critical quantity to be iterated in the solution of the surface heat balance. Surface melting (Δh_s) is a response to the surface heat balance when the surface temperature tends to increase above the freezing point.

(3) The temperature profile in the ice $T_i(z,t)$ is numerically solved from the heat-conduction equation. The upper boundary condition is the surface temperature, and the lower boundary condition is the freezing temperature (T_f) at the ice bottom. Absorption of shortwave radiation $I(z)$ in the snow and ice is an additional source term in the heat-conduction equation. The volumetric heat capacity $(\rho c)_{si}$ and the heat conductivity of sea ice (k_{si}) are functions of ice salinity (s_i) and temperature. In the case of a thin snow cover, $0 < h_s < 0.01$ m, a single snow layer (Q_{si}, h_s) is coupled with ice. For snow thickness of >0.01 m, the heat-conduction equation is also applied to calculate temperatures (T_{snow}) at various depths in the snow. The snow/ice interface temperature (T_{in}) is calculated according to the flux continuation assumption ($F_c = Q_{si}$).

(4) The difference between the heat flux from the ocean mixed layer (F_w) and conduction upwards from the ice bottom (Q_c) determines the ice growth or melt ($\pm\Delta h_i$) at the ice bottom.

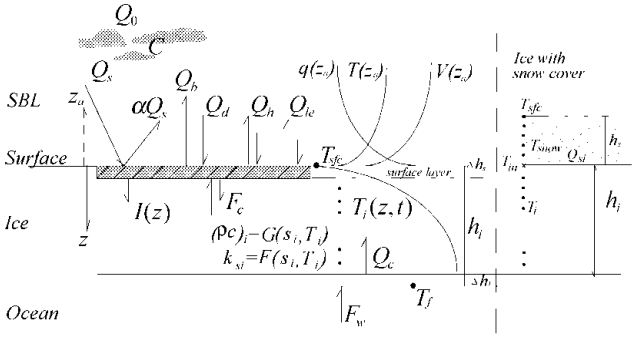

Fig. 1. Structure of the FIMR one-dimensional thermodynamic sea-ice model. For symbols, see the text.

https://doi.org/10.3189/172756401781818536 Published online by Cambridge University Press

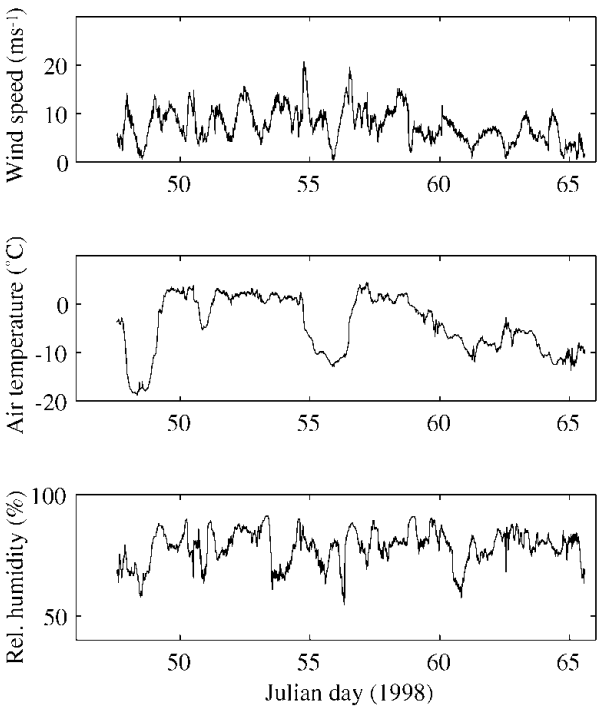

Fig. 2. Time series of wind speed (at 10 m), air temperature (10 m) and moisture (4.6 m) during BASIS.

FIELD DATA AND MODEL PARAMETERS

The BASIS field experiment was carried out from 16 February to 7 March 1998 in the Baltic Sea. The central ice station was located in a coastal fast-ice zone, near the anchored Finnish vessel R/V *Aranda*. Observations of wind speed, air temperature and relative humidity were made from a sea-ice weather mast. The 10 min averages of these quantities served as the forcing data for the ice model. The data time series are shown in Figure 2. Cloudiness (C) was observed visually every 3 hours. Downward and upward shortwave and longwave radiation were measured during BASIS, but 4.2 days of these measurements are missing due to bad weather conditions. Large variations were observed in the surface albedo; the measured shortwave radiation and albedo values were used for the model input. In the case of missing data, R/V *Aranda*'s shortwave radiation measurements and an average albedo of 0.73 were used. A thermistor string with 11 sensors was deployed vertically through the snow and ice. The temperatures of near-surface air, snow, ice and sea water near the ice bottom were measured at various levels. The installation of the thermistor string and its sensors are shown schematically in Figure 3, indicating the initial and final stages in the ice. Snow and ice thickness were measured manually once a day at 10 locations near the thermistor string. The daily means of snow thickness were interpolated linearly and used as model input. A sonic anemometer (Metek) was also deployed, and eddy fluxes of sensible heat and momentum were measured. For a short-period simulation, the model parameters were specified to correspond to the BASIS field characteristics; these are given in Table 1 (note that the salinity of the Baltic Sea ice is much less than that of the sea ice in the oceans). In this study, oceanic heat flux was specified as an input for the model. Eddy-flux measurements performed in the water near the ice bottom suggested that there was, on average, a small upward heat flux (1.0 W m^{-2}) during BASIS. Its small magnitude is explained by the strong water stratification below the ice in the Baltic Sea. In the simulation, we initialized the model with the weather forcing of BASIS and with the observed solar radiation until a stable vertical temperature profile in the snow and ice was achieved.

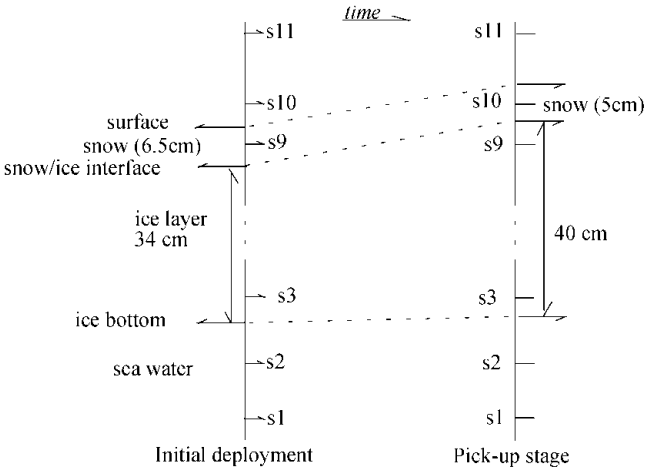

Fig. 3. Geometric location of sensors attached to an ice thermistor string in the air/snow surface, snow/ice interface and ice/water. At the beginning, sensor s10 was 1.5 cm above the surface. The snow depth was 6.5 cm (3 cm soft snow + 3.5 cm hard snow) measured from the surface of the ice. The ice thickness was 34 cm. S3 was 5 cm from the ice bottom. At the end of BASIS, s10 was situated 3.5 cm below the snow surface. The snow/ice interface was 1.5 cm below s10, and the total ice thickness was 40 cm. A distance of 4.5 cm was measured between s3 and the ice bottom.

Table 1. Model parameters based on BASIS measurements and the literature

Aerodynamic roughness (z_0)	10^{-4} m	Launiainen and others (2001)
Extinction coefficient of sea ice (κ_i)	1.5–17 m^{-1}	Modified from Grenfell and Maykut (1977)
Extinction coefficient of snow (κ_s)	25 m^{-1}	Perovich (1996)
Freezing point (T_f)	−0.26°C	$T_f \approx -0.054 s_w$
Sea-ice volumetric heat capacity $(\rho c)_i$	$G(T_i, s_i)$	Maykut and Untersteiner (1971)
Heat capacity of ice (c_i)	2093 J kg^{-1} K^{-1}	
Latent heat of freezing (L_i)	0.33×10^6 J kg^{-1}	
Oceanic heat flux (F_w)	1.0 W m^{-2}	BASIS eddy measurement (average)
Sea-ice density (ρ_i)	910 kg m^{-3}	
Sea-ice salinity (s_i)	0.59–0.75 ppm	BASIS ice-core measurement
Sea-water salinity (s_w)	4.9 ppm	BASIS measurement (average)
Snow density (ρ_s)	310 kg m^{-3}	BASIS measurement (average)
Surface emissivity (ε)	0.97	
Sea-ice heat conductivity (k_{si})	$F(T_i, s_i)$	Maykut and Untersteiner (1971)
Thermal conductivity of ice (k_i)	2.03 W m^{-1} K^{-1}	
Thermal conductivity of snow (k_s)	0.24 W m^{-1} K^{-1}	Calculated according to Yen (1981)
Time-step of model (t)	10 min	
Number of layers in the ice	10	
Number of layers in the snow	5	

RESULTS

The measured downward solar radiation in the midday period showed several large peaks. For comparison, it was

https://doi.org/10.3189/172756401781818536 Published online by Cambridge University Press

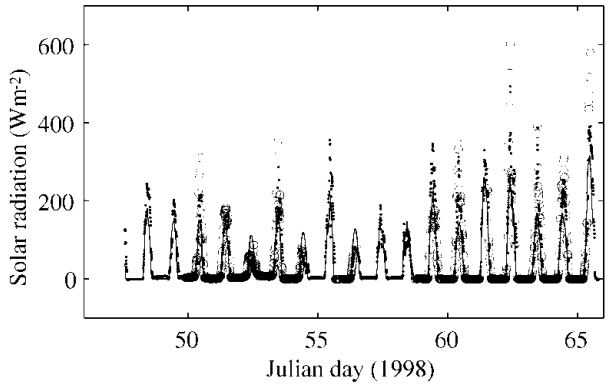

Fig. 4. Measured and estimated shortwave radiation. Circles indicate measurements by the radiometer over the sea ice, and solid dots measurements on the R/V Aranda. *The solid line gives the results calculated using an empirical formula. The model calculations use the measured values.*

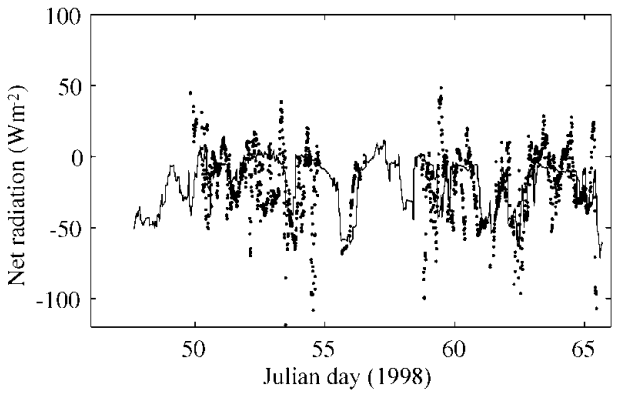

Fig. 5. Net longwave radiation flux comparison. The solid line gives the ice-model estimate, and dots are the observed values.

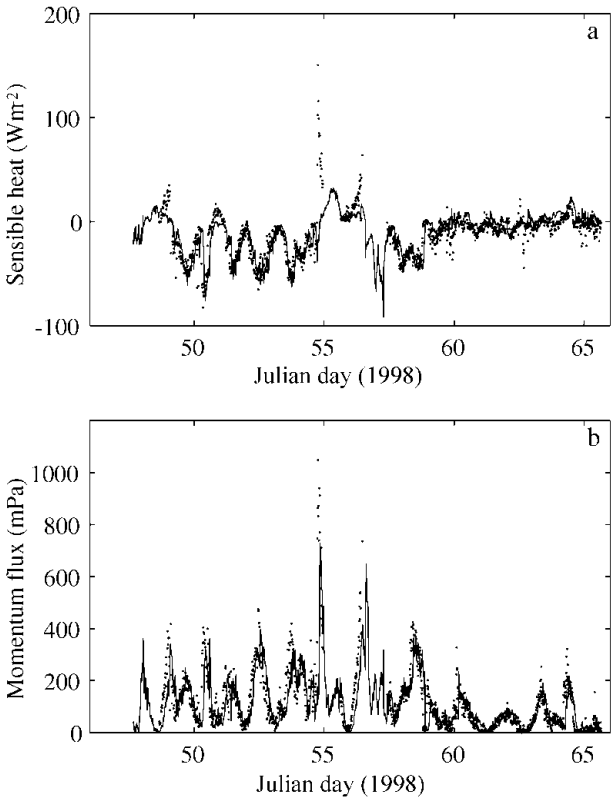

Fig. 6. Modelled (solid line) turbulent surface fluxes of sensible heat (a) and momentum (b) compared with those measured as eddy fluxes by the sonic anemometer (dots).

also calculated (Fig. 4) using an empirical sinusoidal formula taking the observed cloudiness into account, i.e. $Q_s = Q_0(1-0.52C)$, where Q_0 was calculated from Shine's (1984) formula for clear skies, and $(1-0.52C)$ is a cloudiness factor given by Bennett (1982). Differences may be due to multiple scattering between the snow surface and clouds. During the occurrence of the large peaks, the cloud cover was 0.5–1; large peaks were also present in R/V *Aranda*'s shortwave radiation data. According to several authors (Schneider and Dickson, 1976; Shine, 1984; Wendler and Eaton, 1990), neglect of multiple scattering may lead to errors of 30–60% in the surface shortwave radiation flux. Several parameterizations of downward longwave radiation are included in the ice-model code for comparison. The parameterization of Prata (1996), combined with the cloudiness factor of Jacobs (1978), was selected for this study. Comparison of the observed and calculated net longwave radiation flux is shown in Figure 5. Differences were mainly related to the estimation of downward longwave radiation, especially during the period before day 55 when the air temperature was above freezing point and melting was predicted by the model. In the later part of the period, the calculations compare somewhat better with the measurements. A comparison of modelled eddy fluxes of momentum and sensible heat and those measured by the sonic anemometer is shown in Figure 6. The results indicate that the ice model simulates these fluxes quite well. The mean values of the various surface fluxes are given in Table 2. The observed and modelled in-ice temperatures are compared in Figure 7. The thermistor-string measurements indicated snow-ice formation near the surface (Fig. 3). At the beginning of the period, a large vertical gradient is seen in the experimental in-ice temperature profile (Fig. 7a), indicating rapid freezing around the thermistor string after its installation. This was not well simulated by the ice model (Fig. 7b) because the installation of the thermistor string caused water flooding near the surface, which was not taken into account in the model initialization. The modelled average in-ice conductive heat flux was 10.7 W m^{-2} upward, while the thermistor-string measurement indicated an average upward heat flux of 8.1 W m^{-2}. The difference may be due to the inaccuracy of the estimated heat conductivity and the complexities of the snow cover above ice. However, the results (Fig. 7b) still indicate an encouraging agreement

Table 2. Observed and calculated mean values of various surface heat fluxes

	Q_s(down)	Q_s(net)	Q_d	Q_b	$Q_d + Q_b$	Q_{net}	T_{sfc}	Q_h	τ
Observed	50.1	11.1	262.6	−282.2	−19.6	−8.5	−6.3	−10.8	113.5
Calculated	34.0	9.4	270.6	−287.4	−16.8	−7.4	−4.4	−9.9	104.6

https://doi.org/10.3189/172756401781818536 Published online by Cambridge University Press

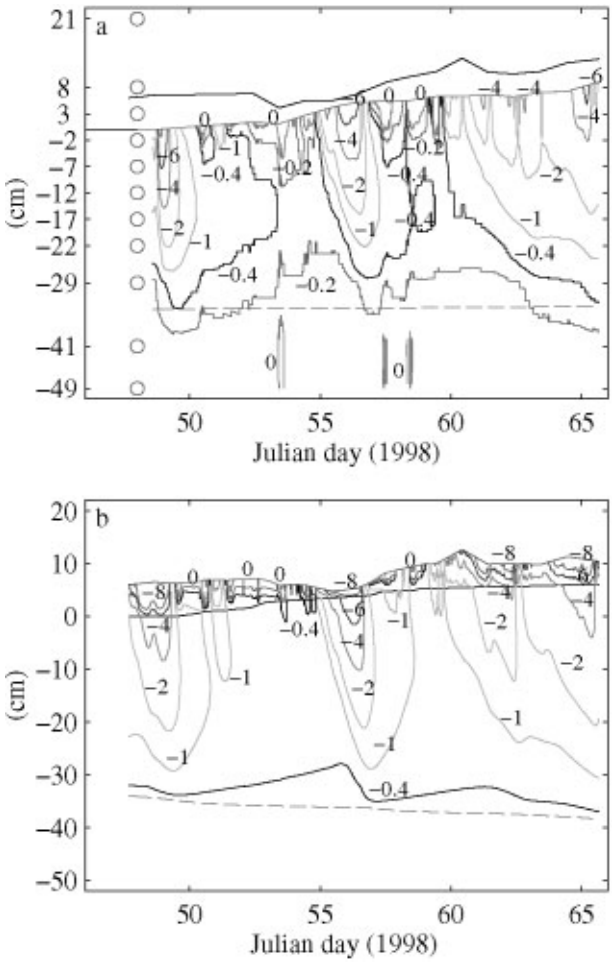

Fig. 7. Internal ice temperatures (°C) during the BASIS experiment. (a) Observed in-ice temperatures. Circles indicate the locations of sensors attached to the thermistor string. (b) In-ice temperatures calculated by the ice model. The three horizontal lines show the average observed (a) and modelled (b) evolution of the height/depth of the snow surface, the snow/ice interface and the ice bottom.

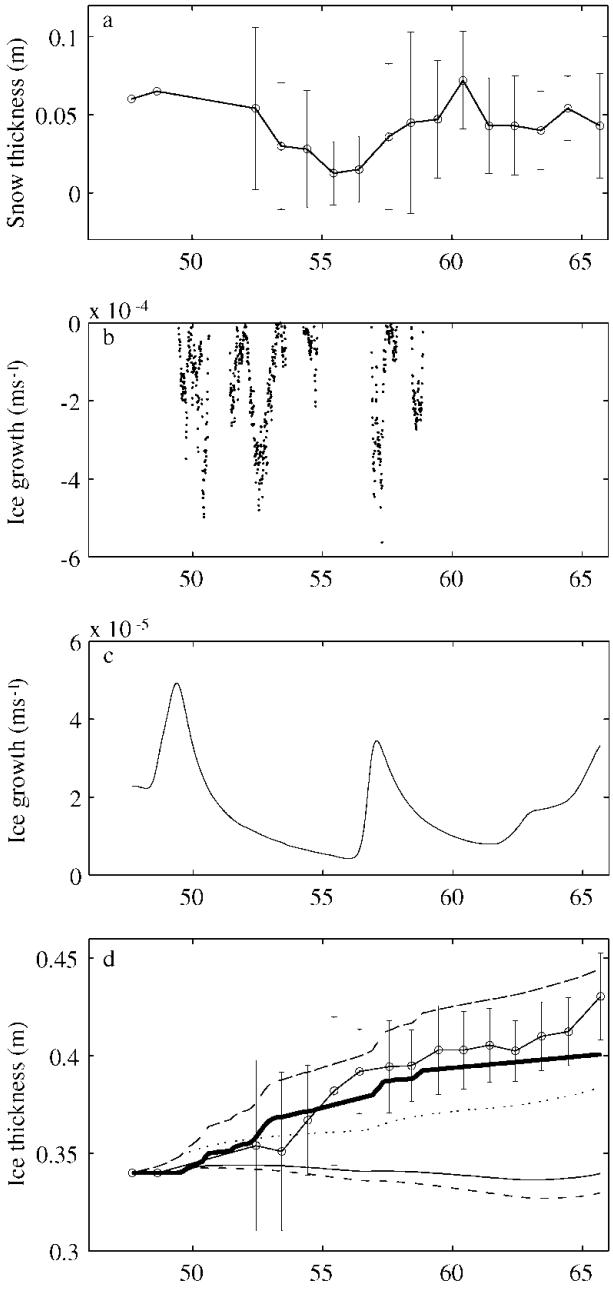

Fig. 8. (a) Observed mean snow thickness (circle-connected line) with ± standard deviation (vertical bars). (b) Modelled melting rate at the surface. (c) Modelled freezing at the ice bottom. (d) Observed mean ice thickness (circle-connected line) with ± standard deviation (vertical bars). The dotted line gives the modelled ice growth at the bottom, and the thick line gives the ice growth solely due to snow/ice transformation. The broken line on top is the cumulative ice growth. The lowermost two lines (solid and broken) give the ice-thickness variation calculated from the ice-bottom heat mass balance using thermistor-string temperature data with an assumed average oceanic heat flux of 1 and 2 W m^{-2}, respectively.

with the observed thermal structure and its time development. The modelled air/snow interface temperature was compared with the radiation measurement-derived surface temperature, and with estimates derived from the flux-profile relationships (Launiainen and others, 2001). The results indicate that the ice model can generally reproduce the surface temperature well. However, in cases of small surface heat fluxes, the surface boundary is flux-controlled in the model, and the modelled surface temperature may be less accurate. The measured snow and ice and modelled ice-thickness variations are shown in Figure 8. The measurements of snow and ice show distinct spatial and temporal variations in the test area, due to highly variable weather during the BASIS experiment. The surface melting largely occurred when measured air temperatures were above freezing. Figure 8b shows the time series of the modelled surface melting, producing a cumulative snow-thickness change of about 12 cm. Figure 8c gives the modelled ice growth at the ice bottom, leading to a 3 cm increase in thickness. Figure 8d shows the simulated ice thickness compared with the measurements. Assuming the surface meltwater is totally refrozen, and the density ratio between the snow and sea ice is 0.35, the above modelled melting would correspond to about 5 cm of snow-ice formation. In practice, however, instead of immediately refreezing, melting water percolates into the snow/ice interface and may be mixed with snow to form a slush layer, which later will be refrozen under the right weather conditions. Such a layer of slush or snow ice will affect the heat conduction and heat flux through the whole ice layer. These uncertainties may cause discrepancies between the measurements and modelling of ice temperature and ice thickness. Further studies on this aspect are needed.

https://doi.org/10.3189/172756401781818536 Published online by Cambridge University Press

Some comparative estimates can be made from the measured ice-thickness and ice-temperature data (Wettlaufer and others, 1990). At the ice bottom, a heat balance is achieved between heat conduction, latent heat of fusion and oceanic heat flux. Accordingly, the heat/mass balance reads: $\rho_i L_i \partial h_i/\partial t = k_i \partial T_i/\partial z - F_w$. The thermistor-string measurements (Fig. 3) indicate an approximate mass equilibrium during BASIS with no effective thickness change at the ice bottom. Using the modelled thermal structure and heat conduction near the ice bottom, this equilibrium corresponds to an average oceanic heat flux of 0.63 W m^{-2}. On the other hand, assuming a small average oceanic heat flux and calculating the heat conduction near the ice bottom from the measured temperature profile, the ice thickness controlled by the bottom heat/mass balance would be in approximate equilibrium for $F_w = 1$ W m^{-2} and indicates a melting of about 1 cm for $F_w = 2$ W m^{-2} (Fig. 8d). The ice equilibrium for $F_w = 1$ W m^{-2} agrees with the ice-thickness measurements by the thermistor string and with the below-ice eddy-flux measurements.

The model input quantities for this simulation showed large temporal variations, especially in solar radiation and surface albedo. The ice model was forced by the observed shortwave radiation, and this produced better results than a control run using the parameterized values. This was concluded from comparisons of the observed and modelled surface temperature and net radiation, which were measured independently of the shortwave radiation. As for the model initialization, if we assume a constant vertical temperature profile of −0.5°C in the ice, the in-ice temperature adjustment would cause a difference in ice-growth rate in the first 2 days of simulation and eventually a 20% change in the overall ice thickness compared with the current model run. In addition, the estimation of the thermal heat conductivities of ice and snow is of primary importance for the modelling of ice thermodynamics. In this study we used a simple parameterization. Potential errors due to this inaccuracy may remain in the model results with respect to the in-ice conductive heat flux. Further data on the heat conductivity are needed.

CONCLUSION

An 18 day ice-model simulation was carried out using the BASIS field data. In general, the overall results of the ice model were encouraging. The in situ field data provided a good opportunity to verify the model parameters and indicated that high-quality field data are a prerequisite for model validation. The air–ice turbulent fluxes were well estimated by the model, indicating an accurate simulation of the air–ice coupling. Results indicate that surface meltwater is an important source for snow-ice formation during a mild winter. The in-ice temperature simulation indicated reasonable agreement of the thermal structure and its time development. Accurate model initialization is important for a short-period simulation of the overall ice thickness. The model slightly overestimated the ice growth at the ice bottom. This may be due to uncertainties in the estimation of sea-ice thermal properties and to the lack of a coupled ocean model.

ACKNOWLEDGEMENTS

We are grateful to the participants in the BASIS-98 field experiment. In particular, K. Shirasawa provided us with his under-ice heat-flux data. The study is part of the European Commission-supported BALTEX-BASIS project under contract MAST3-CT97-0117.

REFERENCES

Bennett, T. J., Jr. 1982. A coupled atmosphere–sea ice model study of the role of sea ice in climatic predictability. *J. Atmos. Sci.*, **39**(7), 1456–1465.

Cheng, B. and J. Launiainen. 1998. A one-dimensional thermodynamic air–ice–water model: technical and algorithm description report. *Meri*, **37**, 15–35.

Ebert, E. E. and J. A. Curry. 1993. An intermediate one-dimensional thermodynamic sea ice model for investigating ice–atmosphere interactions. *J. Geophys. Res.*, **98**(C6), 10,085–10,109.

Gabison, R. 1987. A thermodynamic model of the formation, growth, and decay of first-year sea ice. *J. Glaciol.*, **33**(113), 105–119.

Grenfell, T. C. and G. A. Maykut. 1977. The optical properties of ice and snow in the Arctic Basin. *J. Glaciol.*, **18**(80), 445–463.

Jacobs, J. D. 1978. Radiation climate of Broughton Island. *In* Barry, R. G. and J. D. Jacobs, *eds. Energy budget studies in relation to fast-ice breakup processes in Davis Strait: climatological overview.* Boulder, CO, University of Colorado. Institute of Arctic and Alpine Research, 105–120. (INSTAAR Occasional Paper 26.)

Launiainen, J., *ed.* 1999. *BALTEX-BASIS data report 1998.* Geesthacht, International BALTEX Secretariat. (Publication 14.)

Launiainen, J. and B. Cheng. 1998. Modelling of ice thermodynamics in natural water bodies. *Cold Reg. Sci. Technol.*, **27**(3), 153–178.

Launiainen, J., Cheng Bin, J. Uotila and T. Vihma. 2001. Turbulent surface fluxes and air–ice coupling in Baltic air–sea–ice study (BASIS). *Ann. Glaciol.*, **33** (see paper in this volume).

Maykut, G. A. and N. Untersteiner. 1971. Some results from a time-dependent thermodynamic model of sea ice. *J. Geophys. Res.*, **76**(6), 1550–1575.

Perovich, D. K. 1996. The optical properties of sea ice. *CRREL Monogr.* 96-1.

Prata, A. J. 1996. A new long-wave formula for estimating downward clear-sky radiation at the surface. *Q. J. R. Meteorol. Soc.*, **122**(533), 1127–1151.

Schneider, S. H. and R. E. Dickson. 1976. Parameterization of fractional cloud amounts in climate models. The importance of modelling multiple reflections. *J. Appl. Meteorol.*, **15**(10), 1050–1056.

Shine, K. P. 1984. Parameterization of shortwave flux over high albedo surfaces as a function of cloud thickness and surface albedo. *Q. J. R. Meteorol. Soc.*, **110**(465), 747–764.

Wendler, G. and F. Eaton. 1990. Surface radiation budget at Barrow, Alaska. *Theor. Appl. Climatol.*, **41**(3), 107–115.

Wettlaufer, J. S., N. Untersteiner and R. Colony. 1990. Estimating oceanic heat flux from sea-ice thickness and temperature data. *Ann. Glaciol.*, **14**, 315–318.

Yen, Y.-C. 1981. Review of thermal properties of snow, ice and sea ice. *CRREL Rep.* 81-10.

https://doi.org/10.3189/172756401781818536 Published online by Cambridge University Press